Eur. Phys. J. B **4**, 55–59 (1998)

THE EUROPEAN PHYSICAL JOURNAL B

Melt texturing of $NdBa_2Cu_3O_{7-\delta}$—$Nd_4Ba_2Cu_2O_{10}$ superconductor in short time

N. Hari Babu[1], T. Rajasekharan[1], and V. Seshu Bai[2]

[1] Defence Metallurgical Research Laboratory, Hyderabad, 500058, India
[2] School of Physics, University of Hyderabad, Hyderabad, 500046, India

Received: 3 September 1997 / Revised: 20 December 1997 / Accepted: 22 January 1998

Abstract. We have melt processed $NdBa_2Cu_3O_{7-\delta}$-$Nd_4Ba_2Cu_2O_{10}$ (NdBCO) superconducting composites with various rates of cooling through their peritectic formation temperature. The microstructural studies reveal that the sample processed even with 40 °C/h rate of cooling is built up with aligned microstructure which is necessary for superior transport current and magnetic properties. In the case of $YBa_2Cu_3O_{7-\delta}$, 1 °C/h rate of cooling is necessary to get highly textured microstructure. Magnetic flux profile measurements reveal that even though the intradomain region is well textured and had good transport and magnetic properties, the interdomain region is relatively weak in the fast cooled sample in comparison with slow cooled ones but is much better than that in polycrystalline samples. The results suggest that, the NdBCO superconductor can be melt processed in short time with much better microstructural features in comparison with YBCO system.

PACS. 74.80.Bj Granular, melt-textured, and amorphous superconductors; powders – 74.25.Ha Magnetic properties – 74.60.Jg Critical currents

It is well-known that very slow rate of cooling (1 °C/h) is needed to develop highly textured superconducting matrix in $YBa_2Cu_3O_{7-\delta}$ (Y-123) because of low Yttrium solubility limit in the Ba-Cu-O melt [1]. Thus, it takes a longer time to melt process Y-123 superconductor, which is a drawback and restricts the practical application. High oxygen partial pressure increased the growth rate 2.5 times higher than that the crystal grown under air [2,3]. This high growth rate was mainly attributed to the increased Y-solubility in high oxygen partial pressure. It is found that certain RE-123 type compounds containing the rare earth (RE) element Nd or Sm, possess a high solubility in the Ba-Cu-O melt [1,4]. When they are processed in air a solid solution phase of the form $RE_{1+x}Ba_{2-x}Cu_3O_{7-\delta}$ is formed locally, which is a low T_c phase [5]. Recently Yoo *et al.* [6] melt processed $NdBa_2Cu_3O_{7-\delta}$ (Nd-123) in reduced oxygen partial pressures to suppress low T_c phase formation and obtained a T_c of 95 K and a better bulk J_c. Salama *et al.* [7] directionally solidified the Nd-123 system and could obtain a well textured Nd-123 matrix even with fast pulling rates (50 mm/h). We have examined the texturing of Nd-123 superconductor with various rates of cooling through the peritectic temperature by the melt textured growth process. We report here the results of microstructural investigations, ac susceptibility and the magnetic flux profile measurements.

Presintered powder with the composition $NdBa_2Cu_3O_{7-\delta}$ + 40 mol% $Nd_4Ba_2Cu_2O_{10}$ is processed by the solid state reaction. Pellets of size 15 mm × 15 mm × 10 mm were pressed uniaxially. Each of these pellets was subsequently heated at 980 °C for 2 h, then rapidly heated to 1115 °C (where 123 melts incongruently into $Nd_4Ba_2Cu_2O_{10}$ + Ba-Cu-O Liquid), held for 10 minutes; cooled rapidly to 1050 °C which is just above the peritectic temperature, and cooled at various rates (1, 4, 10, 20, 40 °C/h) through peritectic temperature to 980 °C for the growth of 123 to occur. The whole treatment for all the samples are carried out in Ar atmosphere to suppress the solid solution phase formation. After texturing, these samples were annealed in oxygen atmosphere to obtain the high T_c superconducting phase. An optical microscope with polarized light and the scanning electron microscope were used to investigate the microstructural features. ac susceptibility is measured using a home made ac susceptometer at 33 Hz and magnetic flux profile measurements were made using an ac inductive method suggested by Campbell [8]. In this method a small ac field is superimposed on large dc fields. The maximum applied ac and dc fields are 10 mT and 1 T, respectively. The induced in-phase signal (S) is measured using a lock-in amplifier operated in wide-band mode. The normalized penetration depth p/R is given by $p/R = 1 - \sqrt{-\frac{1}{K}\frac{dS}{dH_{ac}}}$, where R is the radius of the sample, p is the depth to which the magnetic flux penetrates the sample and K is a constant that represents the signal per Gauss, when the sample is in Meissner state. The in-phase signal is measured as a

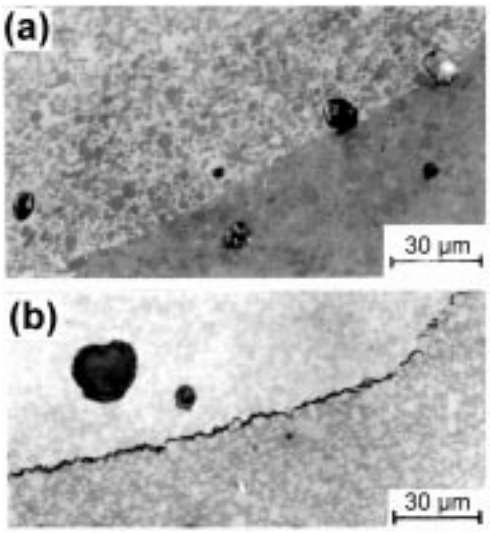

Fig. 1. Microstructures of fast cooled (40 °C/h) sample showing (a) a clean domain boundary and (b) domain boundary with liquid phase.

function of ac field at various fixed dc fields and p/R is calculated from the numerical derivative.

All the samples processed with the rates of cooling 1, 4, 10, 20 and 40 °C/h have well textured domains and showed good levitation and suspension properties to the Nd-Fe-B magnet. The optical microscope with polarized light revealed that the slow cooled (1, 4 and 10 °C/h) samples contained a well textured domains of average size 7−8 mm, and clean domain boundaries without any liquid phase. But the fast cooled (20 and 40 °C/h) samples contained many boundaries with an average domain size of 3−4 mm. Most of the domain boundaries in 40 °C/h cooled sample were clean, *i.e.*, no unreacted Ba-Cu-O liquid phase left out and very few of them have an unreacted liquid phase at the domain boundaries. Optical micrographs of domain boundaries without and with unreacted liquid phase are shown in Figure 1. A boundary that may be contaminated by second phases or other impurities can develop when the boundary is formed as the two domains grow towards one another. When the directions of growth of the two growing domains are normal or nearly normal to the boundary plane between them, impurities and excess solute rejected into the liquid ahead of the growth front can be trapped at the domain boundary, due to insufficient time for the growth of 123. The microstructure of the domain shows presence of two phases one being Nd-123 matrix in the form of platelets separated by gaps and the other insulating phase of fine spherical $Nd_4Ba_2Cu_2O_{10}$ (Nd-422) particles. These particles are uniformly distributed in the Nd-123 matrix. The average size of the Nd-422 particles is found to decrease with increasing cooling rates. Similar observation was reported by Salama *et al.* [7] in directionally solidified samples. Slow cooled samples contained considerable amount of large size acicular Nd-422 particles with average diameter of 4−5 μm and a length of 15 μm as shown in Figure 2a. But in the fast cooled samples, the length of the acicular

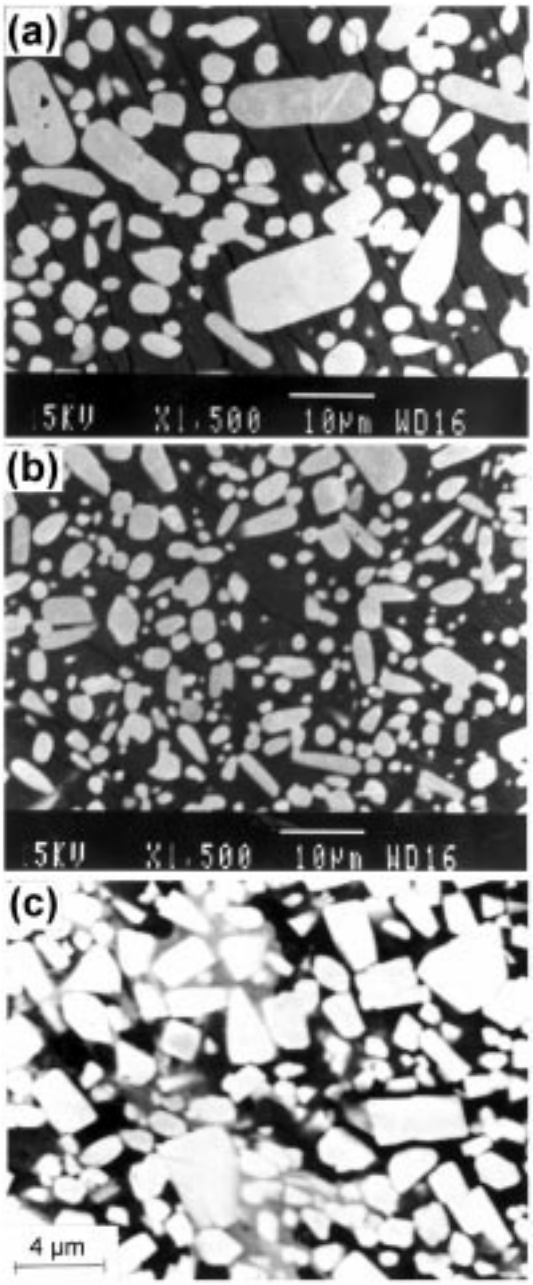

Fig. 2. SEM micrograph of (a) 1 °C/h, (b) 40 °C/h cooled sample, and (c) Quenched microstructure at pro-peritectic stage of Nd-123 with 40 mol % Nd-422 sample.

particles is reduced to 5 μm (Fig. 2b) and also the number of large size acicular particles is less in comparison with the slow cooled samples. Origin of the small sized Nd-422 particles in fast cooled samples can be understood from the microstructure of the sample at pro-peritectic stage *i.e.*, just after decomposition of Nd-123 phase into Nd-422 and liquid phase. It can be seen from the Figure 2c that the average size of the pro-peritectic Nd-422 particles are < 1 μm. Due to higher processing temperatures are involved for Nd-123 system, the size of the pro-peritectic Nd-422 in the liquid increases rapidly with residence time

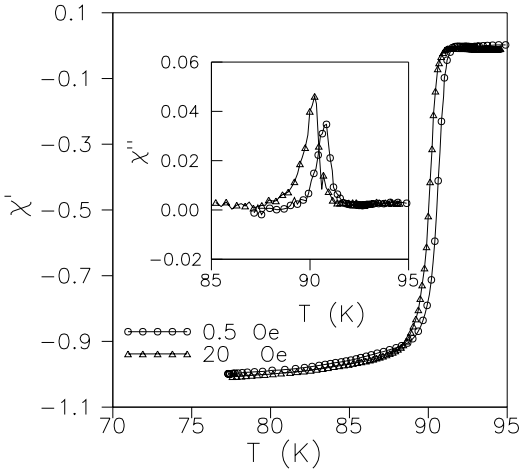

Fig. 3. Real component of ac susceptibility as a function of temperature at two different ac fields. Inset shows the imaginary component.

near peritectic temperature, T_p. Therefore it is difficult to obtain fine Nd-422 particles in the melt processed microstructure with slow rate of cooling. But in the fast cooled samples, the growth of Nd-422 phase in the liquid is suppressed due to low residence time near T_p. The uniformly distributed fine spherical insulating particles are necessary in enhancing the flux pinning [9]. The micro cracks with average size of 0.2 μm observed in the samples are not continuous. The intradomain microstructural features are superior in the fast cooled samples as compared to the slow cooled samples. But the interdomain features in fast cooled (40 °C/h) samples do not seem to be very much favorable to high bulk transport properties. Formation of multidomains is due to the absence of temperature gradient across the sample in the furnace. Single domain can be grown by adopting the seeding technique [10] or by processing the sample in the presence of temperature gradient [11] and thereby the quality of the fast cooled samples can be further improved. In YBCO system, liquid phase segregates at domain boundaries when the cooling rates through T_p exceeds 4 °C/h and also 123 platelets are observed to bend continuously and this hinders planar growth when the cooling rate exceeds 15 °C/h [12]. Absence of liquid phase segregation along the domain boundaries in the NdBCO sample up to 10 °C/h rate of cooling and also presence of the well textured 123 platelets in the sample cooled even at 40 °C/h suggest that the growth rate of NdBCO is one order of magnitude higher than the YBCO system.

Since the superconducting transition temperature is highly sensitive to the processing temperatures, we have measured the T_c of these samples by measuring the ac susceptibility and is shown in Figure 3. The real component of ac susceptibility (χ') showed a sharp diamagnetic transition and the imaginary component (χ'') showed a sharp peak representing the suppression of low T_c phase of $RE_{1+x}Ba_{2-x}Cu_3O_{7-\delta}$. Even though the samples used for these measurements contained many domain boundaries, there was no trace of two transitions in the real part and the two peaks in the imaginary part, suggesting a significant reduction in weak links. Two step behavior is commonly observed in the case of polycrystalline superconductors, where the grains are randomly oriented [13]. The weak dependence of the shift in the ac loss peak (χ''_m) with ac field, represents a high pinning force [14].

Magnetic flux profile measurements at various dc fields in 1, 10 and 40 °C/h rates of cooled samples are shown in Figures 4a, 4b and 4c respectively. The increase of p/R with H_{ac} means that the ac magnetic flux gradually penetrates into the sample with increasing H_{ac} beyond the London penetration depth. The extent of penetration, which is governed by the pinning strength of the material, has increased in the fast cooled samples in comparison with the slow cooled samples. The bulk J_c of a sample can be determined by measuring the slope of flux profile at low H_{ac} fields. A change in slope of the flux profile at high dc fields (marked by arrow), suggests that two different critical current densities are relevant corresponding to the two regions and are considered to be associated with a flux entry initially into the microcracks and then into the platelets from microstructural considerations. This picture is also supported by the High-Resolution Faraday measurements of Schuster *et al.* [15] on melt processed $YBa_2Cu_3O_y$. The first slope can be considered as the transport critical current density J_{c1}, since it is associated with the flux gradient at the cracks and it is given by

$$J_{c1} = \left[dH_{ac}/d(p/R)\right]/R. \tag{1}$$

Beyond the characteristic ac field amplitude at which the ac penetration of fluxoid reaches the center of the bulk specimen through the cracks, there is not much change in the extent of penetration, since it occurs in a local region with large shielding current density. This local critical current density (J_{c2}) can be determined by the slope and is given by

$$J_{c2} = \left[2(dH_{ac}/d(p/R)\right]/P_w \tag{2}$$

where, P_w is the average platelet width. It is of the order of 10^5−10^6 Amp/cm^2 for slow cooled and also for fast cooled samples.

The shift on the p/R axis represents the reversible penetration depth (λ'_e) and is the direct sum of various reversible penetration depths arising from different regions. The possible reversible regions are macrocracks, big voids, weakly coupled domain boundaries and the large extent of $Nd_{1+x}Ba_{2-x}Cu_3O_{7-\delta}$ low T_c phase. Moreover, when the ac fields are small, the flux motion is actually reversible in the pinning well. The reversible penetration depth (λ') due to this reversible fluxoid motion is $(H_{dc}d_i/\mu_o J_{c2})^{1/2}$, where d_i is the interaction distance and is approximately given by $d_i = a_f/\zeta$ in a wide range of magnetic fields. In the above, a_f is the fluxoid spacing and ζ is a constant dependent on the kind of pinning center and takes a value of about 4 for a large and strong pinning center [16]. The estimated value at 1 T field is 10 μm. These melt textured samples have no macro cracks, big voids and are 100% dense. Sharp transition in χ' with onset temperature at 92 K and sharp peak in χ'' represents the suppression of solid solution phase, which is a low T_c phase. Since

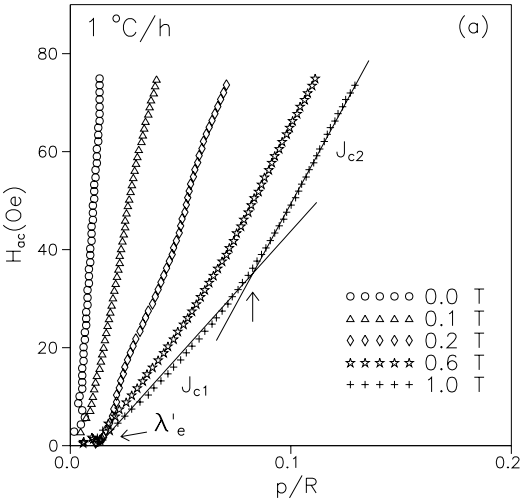

(a)

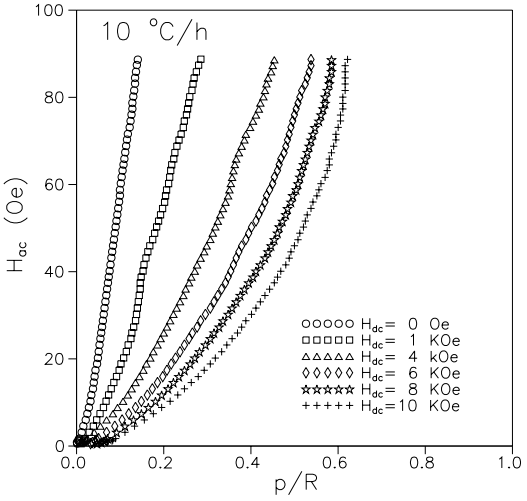

(b)

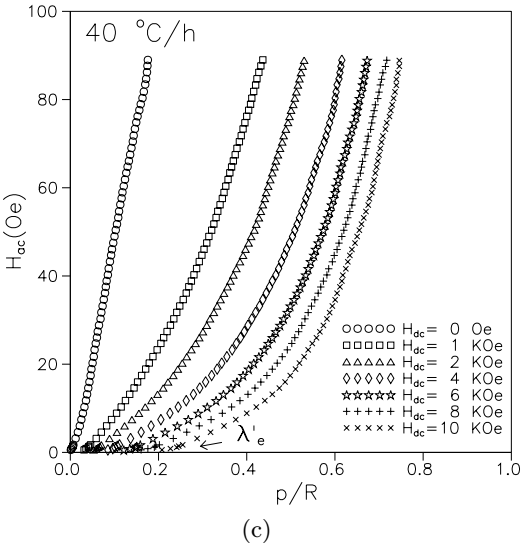

(c)

Fig. 4. Magnetic flux profiles in (a) 1 °C/h, (b) 10 °C/h and (c) 40 °C/h cooled samples.

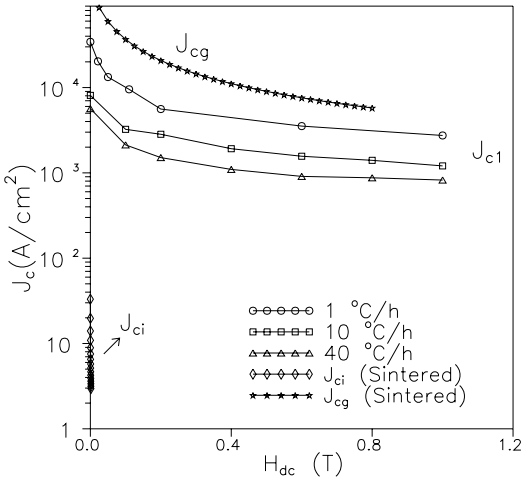

Fig. 5. Bulk J_{c1} of melt textured samples, processed at different cooling rates. The intergranular and intragranular critical current densities J_{ci} and J_{cg} of polycrystalline NdBCO sample are also shown for comparison.

there is no large size regions of low T_c solid solution phase, voids and porosity in these samples, one cannot expect reversible fluxoid motion from these normal regions.

In the slow cooled samples (1, 4 and 10 °C/h) the estimated values of λ' closely match the observed shift (λ'_e) representing the reversible fluxoid motion in the flux pinning potential well. But in the fast cooled (40 °C/h) sample, the observed shift at 1 T field is 100 μm and is considerably larger than the estimated reversible penetration depth of a flux line lattice, which is < 15 μm. Such a large observed shift could be either due to liquid phase at the domain boundaries or due to the weakly coupled domain boundaries. The strong field dependence of reversible penetration depth clearly shows that the observed shift is associated with the domain boundaries that are decoupled at high dc fields, where the ac fluxoids freely moves in and out without getting pinned along the domain boundaries. This is analogous with the reversible flux motion along the grain boundaries in polycrystalline samples [10,17,18]. The measured bulk critical current density of the various fast cooled samples are shown in Figure 5. The bulk critical current density of the fast cooled melt textured sample processed in short time is $\simeq 6000$ A/cm^2, which is 2 orders of the magnitude higher than intergranular critical current density (J_{ci}) in polycrystalline sample. Also the field dependence of J_c is much better, but it is not as good as the samples processed in slow cooling rates. The local current density (J_{c2}) calculated from the slope at higher ac fields is same as that in slow cooled samples. Since the initial chemical composition of the samples used in this study is $NdBa_2Cu_3O_7$ with 40 mol% $Nd_4Ba_2Cu_2O_{10}$, superconducting volume fraction is only 45% in the final microstructure and thereby the lower J_c in comparison with 20−30 mol% added samples, where the superconducting volume fraction is 65−55% [19]. Thus, by optimizing the percentage of Nd-422 content, and by controlling the nucleation of domains using seeding technique, the bulk critical current density and also the other

superconducting properties in fast cooled samples can be further improved. These results suggest that the NdBCO superconductor can be melt processed in short time with much better microstructural features, in comparison with the YBCO system.

The authors are grateful to the Director, DMRL for permission to publish this work. One of the authors (NHB) would like to thank CSIR, New Delhi for providing financial assistance.

References

1. C. Krauns, M. Sumida, M. Tagami, Y. Yamada, Y. Shiohara, Z. Phys. B **96**, 207 (1994).
2. X. Yao, T. Mizukoshi, M. Egami, H. Zama, M. Nakamura, Y. Shiohara, Jpn J. Appl. Phys. **35**, 2126 (1996).
3. X. Yao, T. Mizukoshi, M. Egami, Y. Shiohara, Physica C **263**, 197 (1996)
4. M. Nakamura, H. Kutami, Y. Shiohara, Physica C **260**, 297 (1996).
5. S. Li, E.A. Hayri, K.V. Ramanujachary, M. Greenblatt, Phys. Rev. B **38**, 2450 (1988).
6. S.I. Yoo, M. Murakami, N. Sakai, T. Higuchi, S. Tanaka, Jpn J. Appl. Phys. **33**, L1000 (1994).
7. K. Salama, A.S. Parikh, L. Woolf, Appl. Phys. Lett. **68**, 1993 (1996).
8. A.M. Campbell, J. Phys. C **2**, 1492 (1969).
9. M. Murakami, S. Gotoh, N. Koshizhuka, S. Tanaka, T. Matsushita, S. Kambe, K. Kitazawa, Cryogenics **30**, 390 (1990).
10. V.R. Todt, S. Sengupta, D. Shi, J. Hull, P.R. Sahm, P.G. McGinn, R. Peoppel, J. Electron. Mater. **23**, 1127 (1994).
11. M. Ullrich, H.C. Freyhardt, in *Superconducting Materials*, edited by J. Etourneau, J.B. Torrance, H. Yamauchi, (Gournay-sur-Marne, France: IITT international, 1993), pp. 205-210.
12. E. Sudhakar Reddy, T. Rajasekharan, Phys. Rev. B (in press).
13. N. Hari Babu, T. Rajasekharan, V. Seshu Bai, Phys. Rev. B (in press).
14. K.H. Müller, Physica C **159**, 717 (1989).
15. Th. Schuster, M.R. Koblischka, H. Kuhn, M. Glücker, B. Ludescher, H. Kronmüller, J. Appl. Phys. **74**, 3307 (1993).
16. A.M. Campbell, J. Phys. C **4**, 3186 (1971).
17. H. Küpfer, S.M. Green, C. Jiang, Y. Mei, H.L. Luo, R. Meier-Hirmer, C. Politis, Z. Phys. B **71**, 63 (1988).
18. A. Dang, P.A. Godelaine, Ph. Vanderbemden, R. Cloots, M. Ausloos, J. Appl. Phys. **77**, 3560 (1995).
19. N. Hari Babu, T. Rajasekharan, S. Srinivas, L. Menon, S.K. Malik (to be published).